Electronic Supplementary Material (ESI)

Calix[4]resorcinarene-based [Co_{16}] coordination cages mediated by isomorphous auxiliary ligands for enhanced proton conduction

Ting-Ting Guo,[a] Dong-Ming Cheng,[a] Jin Yang,*,[a] Xianxiu Xu,[b] and Jian-Fang Ma*,[a]

[a]*Key Lab for Polyoxometalate Science, Department of Chemistry, Northeast Normal University, Changchun 130024, People's Republic of China*

[b]*College of Chemistry, Chemical Engineering and Materials Science, Key Laboratory of Molecular and Nano Probes, Ministry of Education, Shandong Normal University, Jinan 250014, People's Republic of China*

* Correspondence authors

E-mail: yangj808@nenu.edu.cn (J. Yang)

E-mail: majf247@nenu.edu.cn (J.-F. Ma)

Fax: +86-431-85098620

Experimental section

Materials and methods. All chemical reagents were available from commercial sources. Thermogravimetric (TG) curves were measured on a Perkin-Elmer TG-7 analyzer under nitrogen gas. Elemental analysis data were determined on a VarioEL III Elemental Analyzer. FT-IR spectra were recorded from KBr pellets on a Mattson Alpha-Centauri spectrometer. Powder X-ray diffraction (PXRD) patterns were determined on a Rigaku SmartLab X-ray diffractometer with graphite monochromatized Cu Kα radiation radiation (λ = 0.154 nm). Mass spectra were conducted on a Bruker autoflexIII smartbeam MALDI-TOF-MS. Gas sorption isotherms were measured on an Autosorb-iQ instrument. Water adsorption isotherms were performed at 298 K on the Autosorb-iQ2 adsorptometer (Quantachrome Instruments).

X-ray crystallography. Single-crystal X-ray diffraction data for **1-SO$_3$H** and **1-OH** were collected on a Bruker D8 VENTURE X-ray diffractometer, using φ and ω scans with MoKα radiation (λ = 0.71073 Å). The structures were solved by direct methods with SHELXS-2013 and refined on F^2 by full-matrix least-squares by using SHELXTL-2013 within WINGX.[S1-S3] Non-hydrogen atoms were refined anisotropically. Hydrogen atoms were generated geometrically. The SQUEEZE routine in PLATON was employed to remove the highly disordered solvents.[S4] Crystallographic data and structure refinement parameters are given in Table S2.

References

(S1) G. M. Sheldrick, *SHELXL-2013, Programs for X-ray Crystal Structure Solution*; University of Göttingen: Göttingen, Germany, 2013.

(S2) G. M. Sheldrick, *SHELXL-2013, Programs for X-ray Crystal Structure Refinement*; University of Göttingen: Göttingen, Germany, 2013.

(S3) L. J. Farrugia, *WINGX: A Windows Program for Crystal Structure Analysis*; University of Glasgow: Glasgow, UK, 1988.

(S4) (S4) A. L. Spek, *Acta Crystallogr., Sect. C: Struct. Chem.*, 2015, **71**, 9.

Proton conductivity measurements. The proton conductivity was measured according to the reported literature.[S1] The samples of **1-SO_3H** and **1-OH** were grounded into a uniform powders with a mortar and pestle, and then were pressed into thin pellets in a mold at 12 MPa for 5 min. The proton conductivity determination was conducted on the IviumStat electrochemical workstation (Netherland) with alternating current (AC) impedance measurements, and the test frequency varied from 1 Hz to 1 MHz under an applied voltage of 50 mV.

Reference

(S1) J.-X. Wang, Y.-D. Wang, M.-J. Wei, H.-Q. Tan, Y.-H. Wang, H.-Y. Zang and Y.-G. Li, *Inorg. Chem. Front.*, 2018, **5**, 1213.

Synthesis of Tetra(2-(1H-pyrazol-3-yl)pyridine)calix[4]resorcinarene (TPC4R-I). The precursors of (**a**)-(**c**) were prepared according to the reported literature.[S1-S3] The synthesis of the precursor (**b**) was similar to that of ***Me*-TPC4R** except that the $BrCH_2Cl$ was replaced by $BrCH_2CH_2Cl$ (Scheme S1).[S1] For the synthesis of **TPC4R-I**, the 2-(1H-pyrazol-3-yl)pyridine (2.591 g, 17.86 mmol) and **(c)** (4.048 g, 3.97 mmol) were added to a stirred suspension of NaOH (1.071 g, 26.79 mmol) in 200 mL dry DMF. Then, the mixture was stirred at 80 °C for 12 h. After the mixture was cooled to room temperature, insoluble impurity was removed by filtration. The solvent was evaporated under vacuum to form a pale yellow solid. The solid was further washed with water and the resulting crude product was crystallized by using CH_2Cl_2-petroleum ether to produce pale yellow powder of **TPC4R-I** in an 86% yield.

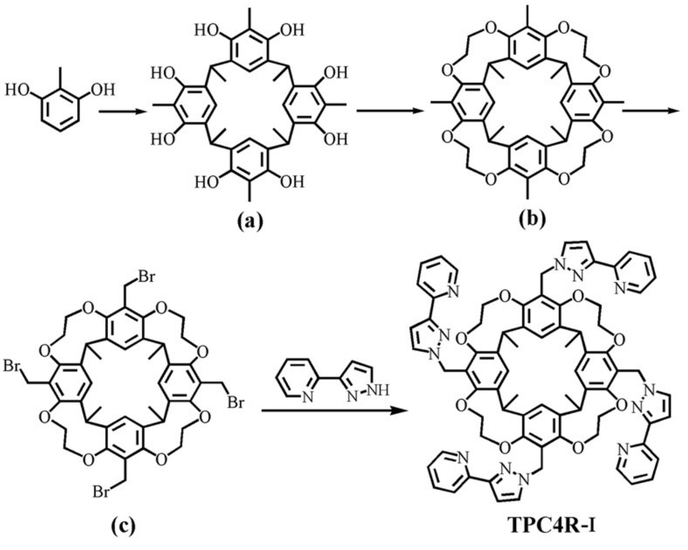

(a)

NaO_3S-H_2L **H_3L1**

(b)

Scheme S1. (a) Synthetic route of cavitand **TPC4R-I** ligand. (b) Isophthalic acid derivatives used in this work.

References

(S1) W.-Y. Pei, G. H. Xu, J. Yang, H. Wu, B. L. Chen, W. Zhou and J.-F. Ma, *J. Am. Chem. Soc.*, 2017, **139**, 7648.

(S2) L. Pirondini, G. Vecchi, S. Negri, A. D. Blasi, C. Massera and E. Dalcanale, *Chem. Commun.*, 2004, **69**, 1362.

(S3) T. N. Sorrell' and F. C. Pigge, *J. Org. Chem.*, 1993, **58**, 784.

Synthesis of $[Co_{16}(TPC4R\text{-}I)_2(HL)_4(L)_8(H_2O)_{24}]\cdot 12DMF\cdot 4H_2O$ (1-SO_3H). A mixture of TPC4R-I (13 mg, 10 mmol), $CoCl_2\cdot 6H_2O$ (15 mg, 50 mmol) and H_3L (15 mg, 60 mmol) was added to a solution of DMF/MeOH (4 mL, 1/1, v/v) in a Teflon reactor (15 mL), to which 150 μL HCl aqueous solution (1.2 M) was added. Then, the reaction mixture was heated at 100 °C for 6 days. After cooling to room temperature, pink diamond-shaped crystals of **1-SO_3H** were achieved in a 55% yield based on TPC4R-I. Element analysis (%) calculated for $C_{284}H_{316}N_{36}O_{140}S_{12}Co_{16}$: C 43.7, H 4.1, N 6.5; found: C 43.1, H 4.7, N 6.9. IR data (KBr, cm^{-1}): 3418 (s), 1611 (s), 1568 (m), 1470 (m), 1440 (m), 1368 (s), 1202 (m), 1103 (m), 1041 (s), 998 (w), 865 (w), 778 (m), 716 (m), 680 (w), 626 (s), 457 (w).

Synthesis of $[Co_{16}(TPC4R\text{-}I)_2(HL1)_4(L1)_8(H_2O)_{16}]\cdot 17DMA\cdot H_2O$ (1-OH). A mixture of TPC4R-I (13 mg, 10 mmol), $CoCl_2\cdot 6H_2O$ (15 mg, 50 mmol) and H_3L1 (10 mg, 60 mmol) was added to a solution of DMA/MeOH (4 mL, 1/1, v/v). The resulting suspension was sealed in a Teflon reactor (15 mL) and heated at 90 °C for 3 days. After cooling to room temperature, deep purple diamond-shaped crystals of **1-OH**

were achieved in a 49% yield based on TPC4R-I. Element analysis (%) calculated for $C_{316}H_{363}N_{41}O_{110}Co_{16}$: C 51.0, H 4.9, N 7.7; found: C 51.5, H 5.1, N 7.2. IR data (KBr, cm^{-1}): 3386 (s), 1613 (s), 1440 (s), 1384 (s), 1274 (m), 1223 (m), 1158 (w), 1132 (w), 1102 (m), 1061 (m), 1020 (m), 1003 (w), 977 (w), 895 (w), 864 (w), 782 (s), 722 (m), 597 (m), 478 (w).

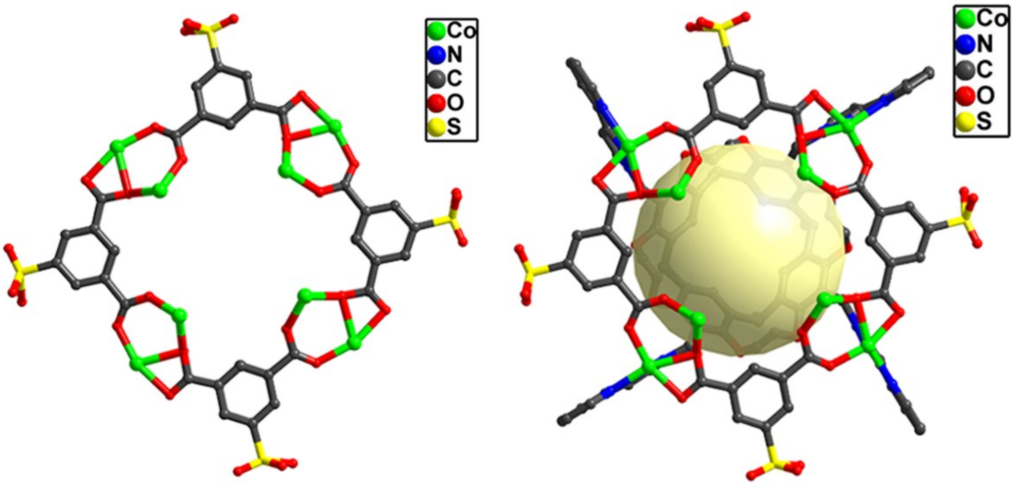

(a) (b)

Fig. S1. (a) View of the $[Co_8(L)_4]^{4+}$ macrocycle in **1-SO₃H**. (b) View of the Co(II)-coordinated calix[4]resorcinarene cavitand $[Co_8(TPC4R\text{-}I)(L)_4]^{4+}$ in **1-SO₃H**.

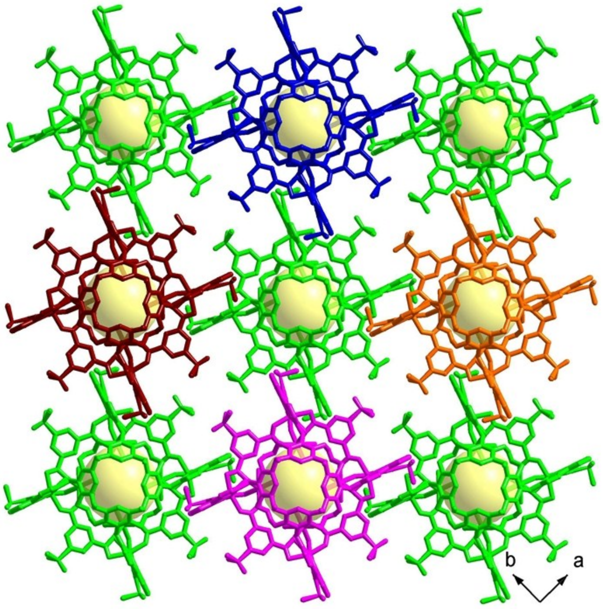

(a)

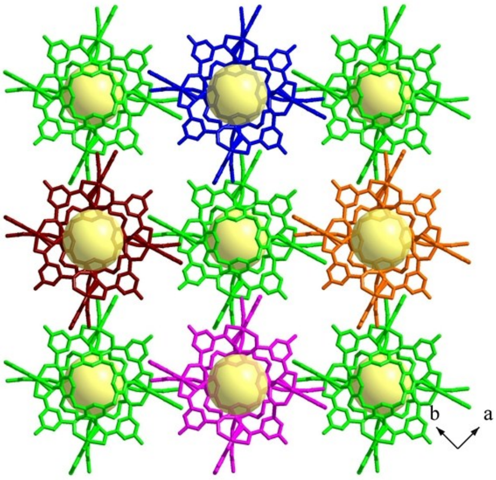

(b)

Fig. S2. 3D porous supramolecular architectures stabilized by π-π interactions for **1-SO$_3$H** (a) and **1-OH** (b).

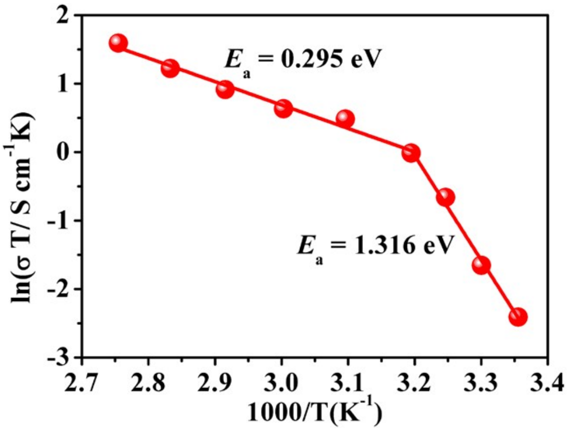

(a)

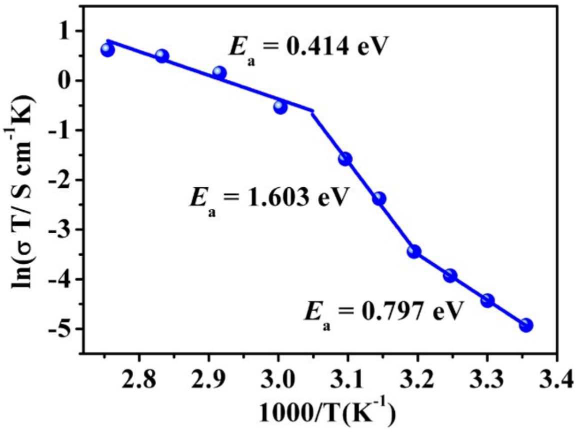

(b)

Fig. S3. Arrhenius plot of proton conductivity under 98% RH for **1-SO$_3$H** (a) and **1-OH** (b).

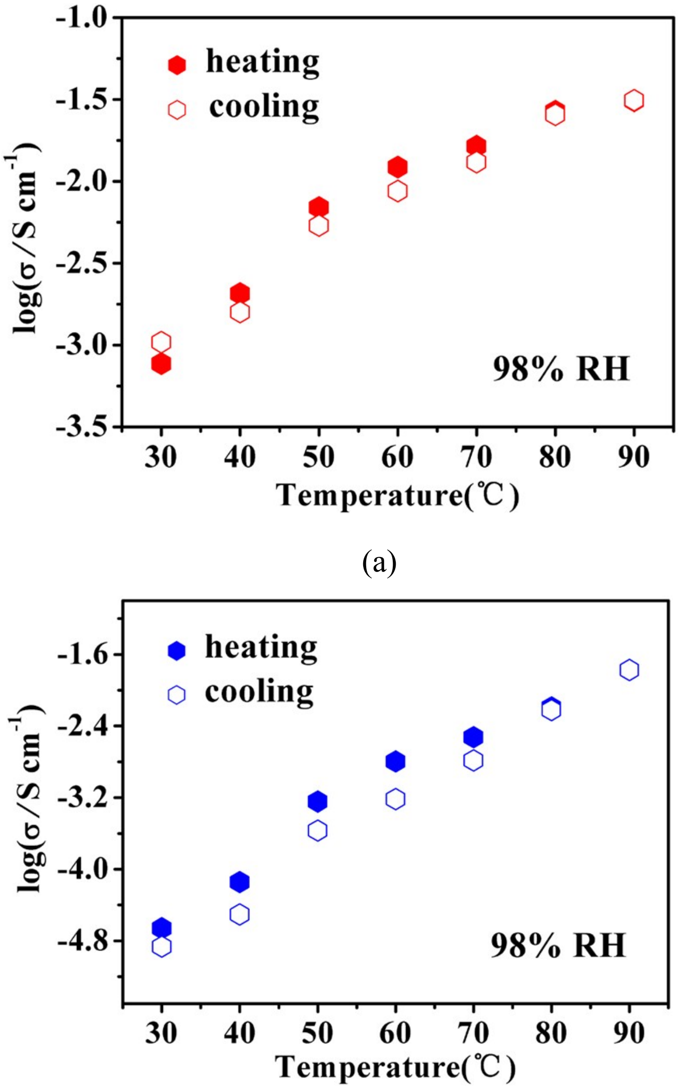

(a)

(b)

Fig. S4. Temperature dependence of the proton conductivities at 98% RH in terms of heating-cooling cycles for **1-SO$_3$H** (a) and **1-OH** (b).

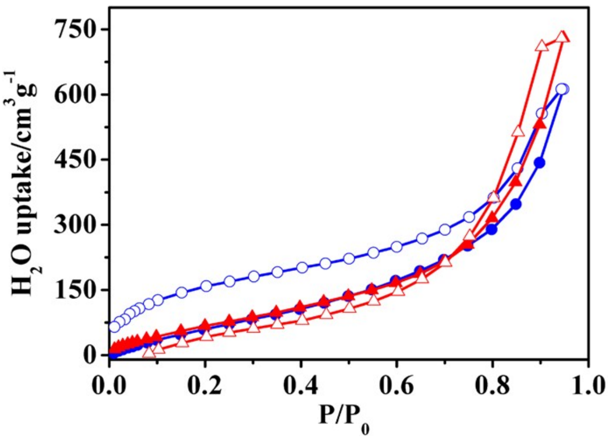

(a)

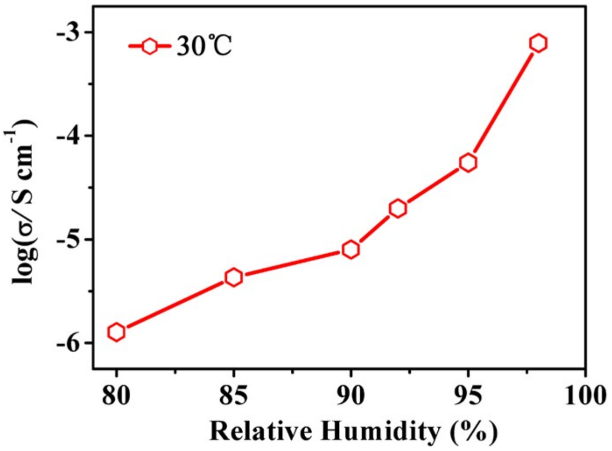

(b)

Fig. S5. (a) Water adsorption (filled circle) and desorption (open circle) isotherms for **1-SO$_3$H** (red) and **1-OH** (blue) at 25 °C. (b) Dependence of proton conductivity on RHs for **1-SO$_3$H** at 30 °C.

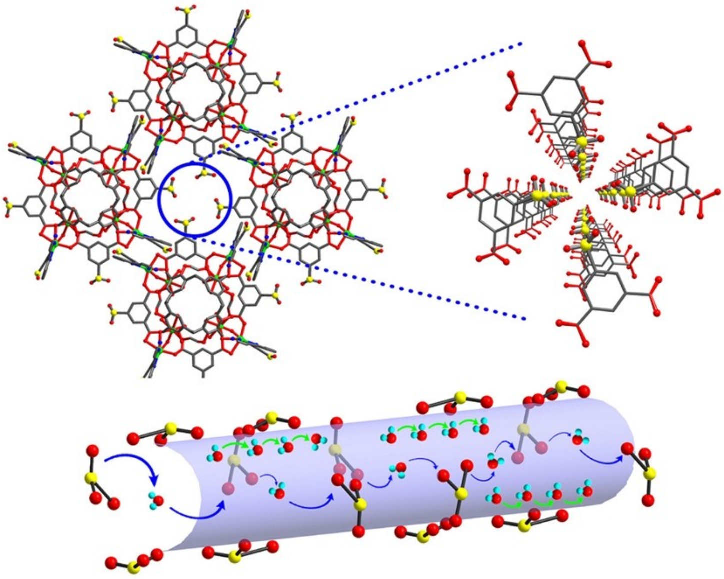

Fig. S6. Schematic representative of possible proton-conducting pathways in the channel formed by adjacent cages of **1-SO$_3$H**. Blue arrows display the protons hop along hydrogen bonds formed by sulfonic acids and absorbed waters. Green arrows show the transport of protons through the protonated water self-diffusion.

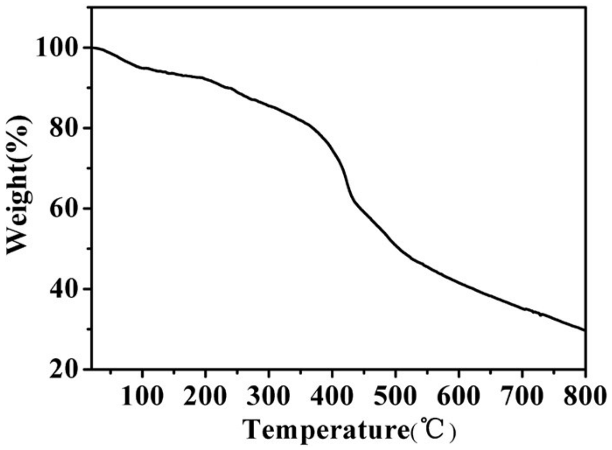

(a)

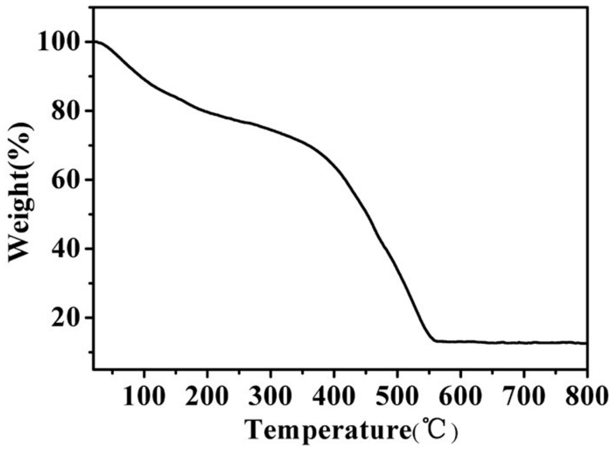

(b)

Fig. S7. Thermogravimetric curves for **1-SO$_3$H** and **1-OH**. TG analyses were conducted under nitrogen gas from 30 to 800 ˚C. For **1-SO$_3$H**, the weight loss of 18% before 341˚C corresponds to the loss of twelve uncoordinated DMF molecules, four uncoordinated water molecules and twenty-four coordinated water molecules. For **1-OH**, the weight loss of 24% before 254 ˚C was attributed to the removal of seventeen uncoordinated DMF molecules, one uncoordinated water molecule and sixteen coordinated water molecules.

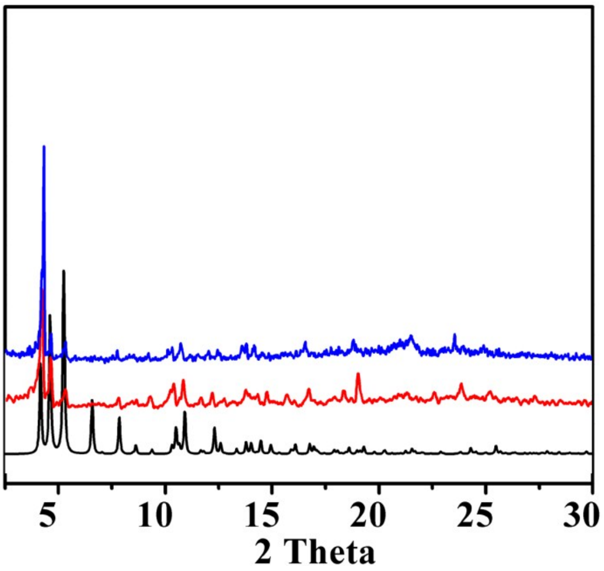

Fig. S8. The simulated (black), experimental (red) and re-solvated (blue) PXRD patterns for **1-SO$_3$H**.

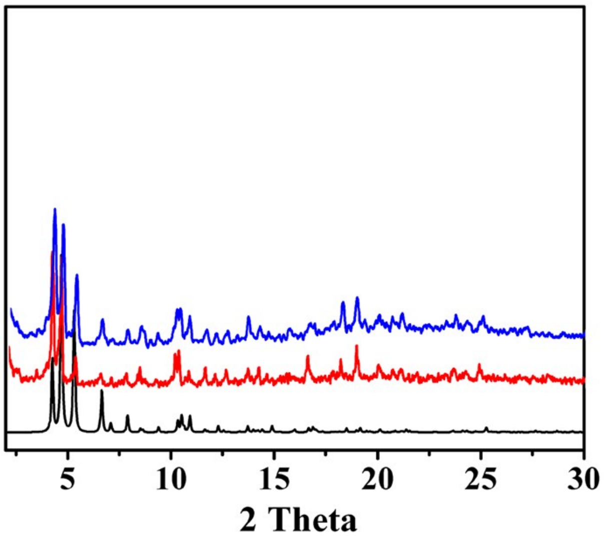

Fig. S9. The simulated (black), experimental (red) and re-solvated (blue) PXRD patterns for **1-OH**.

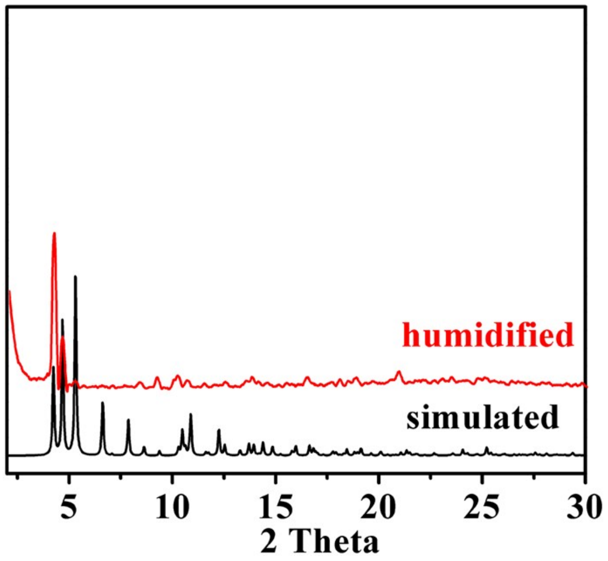

(a)

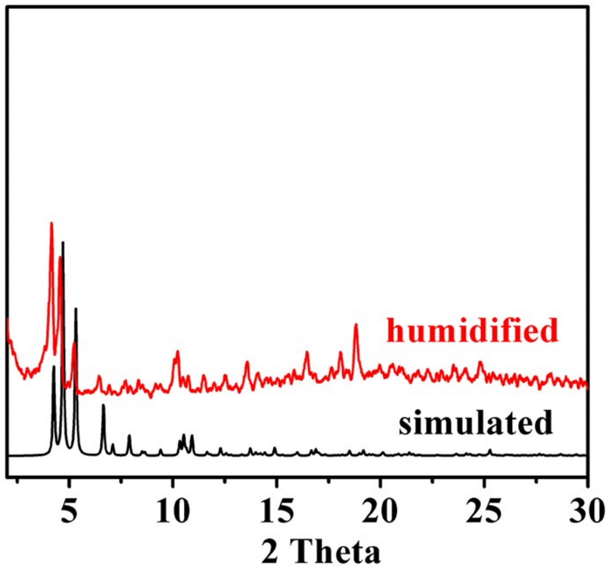

(b)

Fig. S10. PXRD patterns for **1-SO_3H** (a) and **1-OH** (b) under 98% RH.

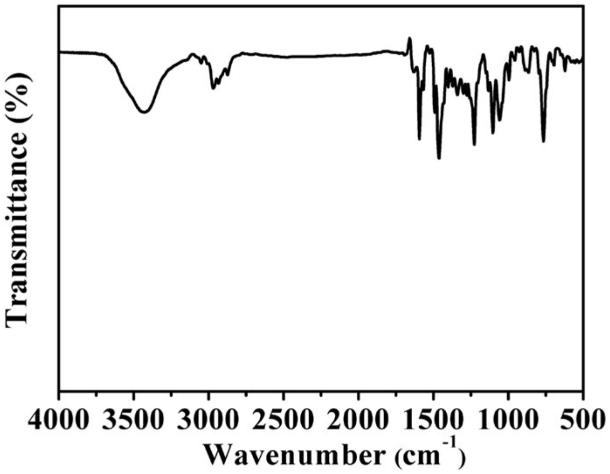

(a)

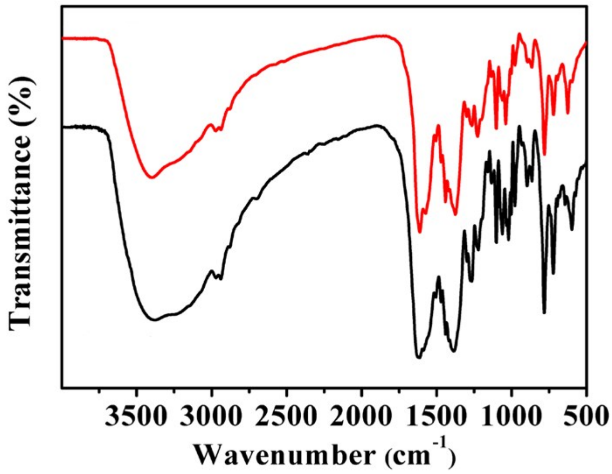

(b)

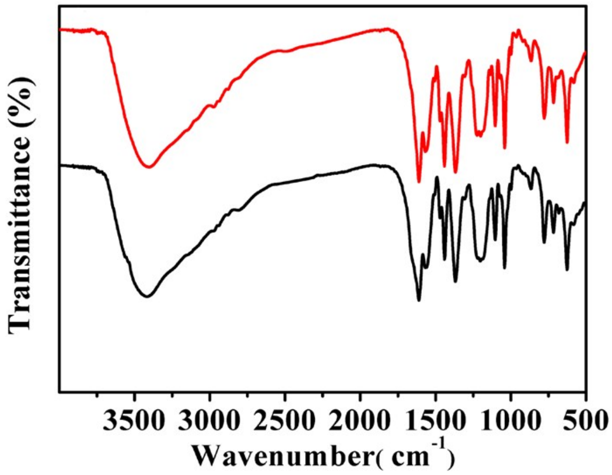

(c)

Fig. S11. (a) IR spectra of **TPC4R-I**. (b) IR spectra of **1-SO$_3$H** (black) and after proton conduction (red). (c) IR spectra of **1-OH** (black) and after proton conduction (red).

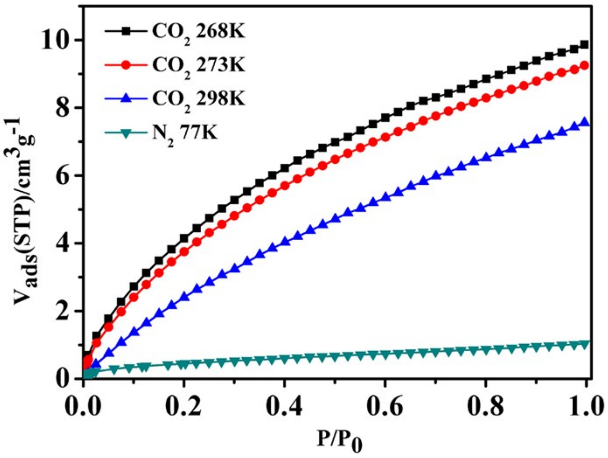

(a)

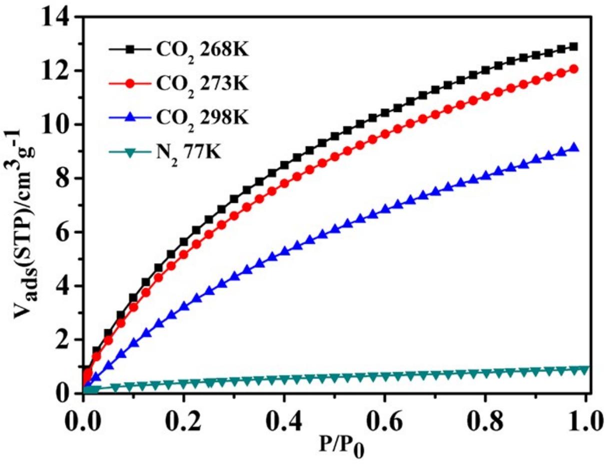

(b)

Fig. S12. Crystalline samples of **1-SO_3H** and **1-OH** were activated in acetone for three days and then heated at 80 °C for 10 h in a vacuum. They exhibit a small CO_2 uptake. The CO_2 adsorptions reach maximum uptakes of 9.86 cm^3(STP)/g for **1-SO_3H** and 12.89 cm^3(STP)/g for **1-OH** at 268 K.

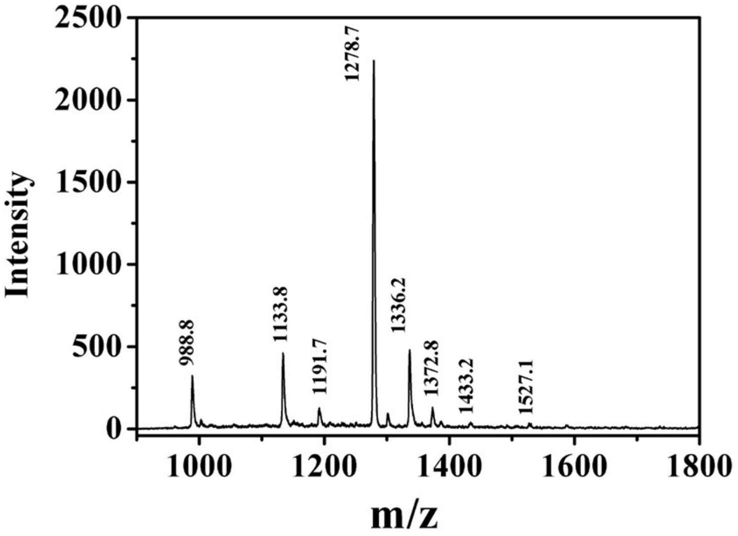

Fig. S13. ESI-MS spectrum of **1-SO_3H** after proton conduction measurement.

Mass fragment table for **1-SO_3H**. $M = Co_{16}C_{248}H_{224}N_{24}O_{124}S_{12} = 6852.28$.

Formula	Change *z*	Calculate *m/z*	Experimental *m/z*
$(M+7H^+)+2MeOH$	7+	989.1	988.8
$(M+7\ H^+)+6MeOH+49H_2O$	7+	1133.3	1133.8
$(M+6\ H^+)+4MeOH+9H_2O$	6+	1191.7	1191.7
$(M+6\ H^+)+13MeOH+22H_2O$	6+	1278.4	1278.7
$(M+6\ H^+)+16MeOH+36H_2O$	6+	1336.4	1336.2
$(M+6\ H^+)+25MeOH+32H_2O$	6+	1372.4	1372.8
$(M+5\ H^+)+4MeOH+10H_2O$	5+	1433.1	1433.2

$(M+5H^+)+12MeOH+22H_2O$	5+	1527.5	1527.1

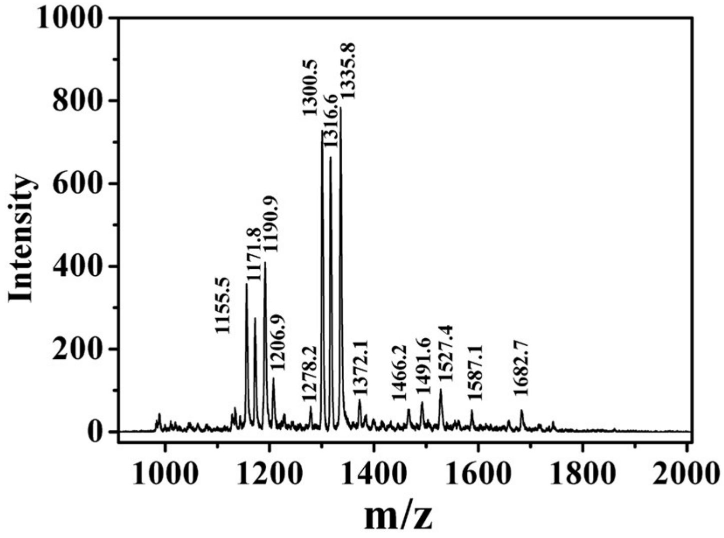

Fig. S14. ESI-MS spectrum of **1-OH** after proton conduction measurement.

Mass fragment table for **1-OH**. $M = Co_{16}C_{248}H_{232}N_{24}O_{92} = 5939.420$.

Formula	Change *z*	Calculate *m/z*	Experimental *m/z*
$(M+6H^+)+10MeOH+37H_2O$	6+	1155.2	1155.5
$(M+6H^+)+17MeOH+30H_2O$	6+	1171.6	1171.8
$(M+6H^+)+16MeOH+38H_2O$	6+	1190.2	1190.9
$(M+5H^+)+9MeOH+15H_2O$	5+	1300.5	1300.5
$(M+5H^+)+7MeOH+23H_2O$	5+	1316.5	1316.6
$(M+5H^+)+6MeOH+30H_2O$	5+	1335.3	1335.8
$(M+5H^+)+9MeOH+61H_2O$	5+	1466.1	1466.2
$(M+4H^+)+4MeOH+2H_2O$	4+	1526.9	1527.4
$(M+4H^+)+6MeOH+33H_2O$	4+	1682.4	1682.7

To certify the cage stability of **1-SO$_3$H** and **1-OH**, the following experiments were conducted. On one hand, the samples were activated at 90 ^{o}C in vacuum for 8 h. Their X-ray diffraction peaks after activation completely disappeared, but the PXRD peaks could be recovered when they were soaked in the mother liquors, indicating that the discrete cage structures were not damaged (Figs. S8 and S9). On the other hand, the samples were maintained at 98% RH for 20 h, and then were dried and soaked into the mother liquors. Their PXRD peaks were also recovered, demonstrating their structural integrity (Fig. S10). Further, the ESI-MS and IR spectra of the samples after proton conduction measurements were used to demonstrate the structural integrity of the discrete coordination cage (Figs. S11, S13 and S14). This similar method has been applied to characterize the structural integrity of the discrete cage in the reported documents (*Angew. Chem. Int. Ed.*, 2018, 57, 5283; *Chem. Sci.*, 2019, 10, 3529 and *J. Am. Chem. Soc.*, 2018, 140, 6271).

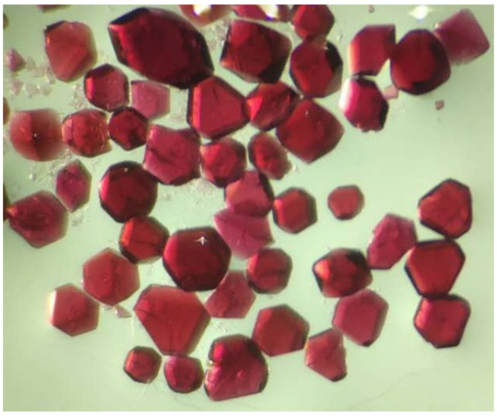

(a)

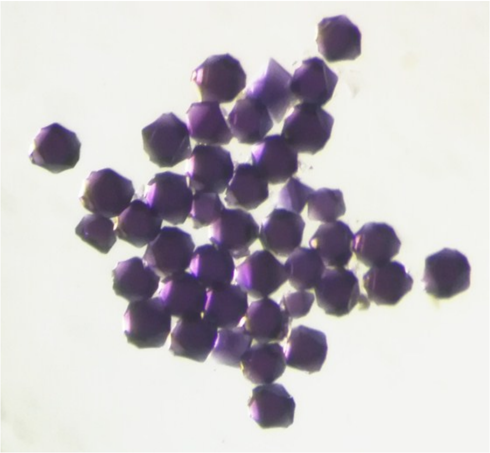

(b)

Fig. S15. Photographs of crystal samples of **1-SO$_3$H (**a**)** and **1-OH** (b).

Table S1. Comparison of proton conductivity of **1-SO$_3$H** and **1-OH** with MOFs.

	compound	RH (%)	T (°C)	conductivity (Scm^{-1})	references
1	**Nafion**	98	80	10^{-1}–10^{-2}	S1
2	**Co-tri**	98	80	1.49 x 10^{-1}	S2
3	**UiO-66$(SO_3H)_2$**	90	80	8.4 x 10^{-2}	S3
4	**$\{H[(N(CH3)_4)_2][Gd_3(NIPA)_6]\}3\ H_2O$**	98	75	7.17 x 10^{-2}	S4
5	**PCMOF-10**	98	70	3.55 x 10^{-2}	S5
6	**KAUST-7’**	95	90	2.0 x 10^{-2}	S6
7	**PCMOF$_2$1/2**	90	85	2.1 x 10^{-2}	S7
8	**H+@$Ni_2(dobdc)(H_2O)_2$ (pH = 2.4)**	95	80	1.9 x 10^{-2}	S8
9	**Im@(NENU-3)**	90	70	1.82 x 10^{-2}	S9
10	**1-SO_3H**	98	90	1.35 x 10^{-2}	This work
11	**Im-Fe-MOF**	98	60	1.21 x 10^{-2}	S10
12	**H_2SO_4@ MIL-101**	0.13	150	1.0 x 10^{-2}	S11
13	**H_3PO_4@MIL-101**	1.1	140	1.0 x 10^{-2}	S11
14	**CPM-103a (50 Mpa)**	98	22.5	0.23 x 10^{-2}	S12
15	**CPM-103b (50 Mpa)**	98	22.5	0.21 x 10^{-2}	S12
16	**1-OH**	98	90	5.10 x 10^{-3}	This work
17	**2-Hmim·$Ga_2F(HPO_3)_3(H_2O)\cdot 0.5H_2O$**	98	85	2.74 x 10^{-3}	S13
18	***β*-PCMOF2**	90	85	1.3 x 10^{-3}	S14
19	**JXNU-2(Sm)**	98	80	1.11 x 10^{-3}	S15
20	**$(H_3O)[Ni^{III}(cyclam)][Ru^{II}(CN)_6]$**	100	22	1.09 x 10^{-3}	S16
21	**$\{(H_3O)[Tb(BODSDC)\text{-}(H_2O)_2]\}_n$**	95	85	6.57 x 10^{-4}	S17
22	**PCMOF**	98	25	3.50 x 10^{-5}	S18

23	**MIL-53(Al)-NH_2**	95	80	4.1 x 10^{-8}	S19

References

(S1) X. Wu, X. Wang, G. He and J. Benziger, *J. Polym. Sci.*, *Part B: Polym. Phys.*, 2011, **49**, 1437.

(S2) M. E. Syed, C. Santanu, W. H. Deng, P. Arun and C. D. Madhab, *Angew. Chem., Int. Ed.*, 2018, **57**, 6662.

(S3) W. J. Phang, H. Jo, W. R. Lee, J. H. Song, K. Yoo, B. Kim and C. S. Hong, *Angew. Chem., Int. Ed.*, 2015, **54**, 5142.

(S4) X.-S. Xing, Z.-H. Fu, N.-N. Zhang, X.-Q. Yu, M.-S. Wang and G.-C. Guo, *Chem. Commun.,* 2019, **55**, 1241.

(S5) P. Ramaswamy, N. E. Wong, B. S. Gelfand and G. K. H. Shimizu, *J. Am. Chem. Soc.*, 2015, **137**, 7640.

(S6) P. G. M. Mileo, K. Adil, L. Davis, A. Cadiau, Y. Belmabkhout, H. Aggarwal, G. Maurin, M. Eddaoudi and S. Devautour-Vinot, *J. Am. Chem. Soc.*, 2018, **140**, 13156.

(S7) S. Kim, K. W. Dawson, B. S. Gelfand, J. M. Taylor and G. K. H. Shimizu, *J. Am. Chem. Soc.*, 2013, **135**, 963.

(S8) W. J. Phang, W. R. Lee, K. Yoo, D. W. Ryu, B. Kim and C. S. Hong, *Angew. Chem. Int. Ed.,* 2014, **53**, 8383.

(S9) Y. Ye, W. Guo, L. Wang, Z. Li, Z. Song, J. Chen, Z. Zhang, S. Xiang and B. Chen, *J. Am. Chem. Soc.*, 2017, **139**, 15604.

(S10) F. M. Zhang, L. Z. Dong, J. S. Qin, W. Guan, J. Liu, S. L. Li, M. Lu, Y. Q. Lan, Z. M. Su and H. C. Zhou, *J. Am. Chem. Soc.*, 2017, **139**, 6183.

(S11) V. G. Ponomareva, K. A. Kovalenko, A. P. Chupakhin, D. N. Dybtsev, E. S. Shutova and V. P. Fedin, *J. Am. Chem. Soc.,* 2012, **134**, 15640.

(S12) Q. G. Zhai, C. Y. Mao, X. Zhao, Q. P. Lin, F. Bu, X. T. Chen, X. H. Bu and P. Y. Feng, *Angew. Chem. Int. Ed.*, 2015, **54**, 7886.

(S13) T. Li, X. J. Qi, J. Li, H. M. Zeng, G. H. Zou and Z. Lin, *Inorg. Chem.*, 2018, **57**, 14031.

(S14) S. Kim, K. W. Dawson, B. S. Gelfand, J. M. Taylor and G. K. Shimizu, *J. Am. Chem. Soc.*, 2013, **135**, 963.

(S15) L. J. Zhou, W. H. Deng, Y. L. Wang, G. Xu, S. G. Yin and Q. L. Liu, *Inorg. Chem.*, 2016, **55**, 6271.

(S16) R. Mateusz, N. Beata, N. Christian, K. Marcin, N. Koji, O. Shin-ichi and S. Barbara, *Inorg. Chem.*, 2018, **57**, 13415.

(S17) W. W. Zhang, Y. L. Wang, Q. Y. Liu and Q. Y. Liu, *Inorg. Chem.*, 2018, **57**, 7805.

(S18) M. Taylor Jared, K. M. Roger; L. M. lgor, I. R. Christopher, V. Ramanathan and K. H. S. George, *J. Am. Chem. Soc.*, 2010, **132**, 14055.

(S19) A. Shigematsu, T. Yamada and H. Kitagawa, *J. Am. Chem. Soc.* 2011, **133**, 2034.

Table S2. Crystallographic data for **1-SO_3H** and **1-OH**.

Compound	**1-SO_3H**	**1-OH**
Formula	$C_{284}H_{316}N_{36}O_{140}S_{12}Co_{16}$	$C_{316}H_{363}N_{41}O_{110}Co_{16}$
Mr	7801.31	7438.33
Temperature (K)	173(2)	173(2)
Crystal system	Tetragonal	Tetragonal
Space group	*I*4/*m*	*I*4/*m*
a (Å)	26.657(12)	26.573(9)
b (Å)	26.657(12)	26.573(9)
c (Å)	33.26(4)	33.219(2)
α(°)	90.00	90.00
β(°)	90.00	90.00
γ(°)	90.00	90.00
V(Å$_3$)	23638(38)	23456(2)
Z	2	2
*D*calc (g·cm^{-3})	1.096	1.053
F(000)	8032	7716
*R*int	0.1430	0.0902
GOF on F^2	1.231	1.299
*R*1, *wR2* [I>2σ(I)]	0.1572, 0.3633	0.1395, 0.3639
*R*1, *wR*2 (all data)	0.3544, 0.4084	0.2397, 0.3994

$^aR_1 = \sum||F_o| - |F_c||/\sum|F_o|$, $wR_2 = \{\sum w[(F_o)^2 - (F_c)^2]^2/\sum w[(F_o)^2]^2\}^{1/2}$

Table S3. Selected bond distances (Å) and angles (deg) for **1-SO_3H**.

Co(1)-O(7)	2.076(10)	O(4)-Co(1)-O(1W)	90.3(4)
Co(1)-O(3W)	2.086(12)	O(7)-Co(1)-O(2W)	89.2(4)
Co(1)-O(6)	2.091(8)	O(3W)-Co(1)-O(2W)	91.1(5)
Co(1)-O(4)	2.174(10)	O(6)-Co(1)-O(2W)	177.0(4)
Co(1)-O(1W)	2.248(14)	O(4)-Co(1)-O(2W)	84.7(4)
Co(1)-O(2W)	2.313(14)	O(1W)-Co(1)-O(2W)	93.4(5)
Co(2)-O(5)	1.981(9)	O(5)-Co(2)-O(8)	93.1(4)
Co(2)-O(8)	1.990(12)	O(5)-Co(2)-O(3)	92.8(4)
Co(2)-O(3)	2.163(11)	O(8)-Co(2)-O(3)	160.4(4)
Co(2)-N(1)	2.167(8)	O(5)-Co(2)-N(1)	92.9(4)
Co(2)-N(2)	2.195(9)	O(8)-Co(2)-N(1)	94.4(4)
Co(2)-O(4)	2.298(8)	O(3)-Co(2)-N(1)	103.9(4)
O(7)-Co(1)-O(3W)	89.8(6)	O(5)-Co(2)-N(2)	169.6(4)
O(7)-Co(1)-O(6)	93.6(4)	O(8)-Co(2)-N(2)	91.9(3)
O(3W)-Co(1)-O(6)	87.9(4)	O(3)-Co(2)-N(2)	85.5(3)
O(7)-Co(1)-O(4)	91.7(4)	N(1)-Co(2)-N(2)	77.6(4)
O(3W)-Co(1)-O(4)	175.5(5)	O(5)-Co(2)-O(4)	92.5(3)
O(6)-Co(1)-O(4)	96.3(3)	O(8)-Co(2)-O(4)	103.6(4)
O(7)-Co(1)-O(1W)	176.8(4)	O(3)-Co(2)-O(4)	57.5(3)
O(3W)-Co(1)-O(1W)	88.4(6)	N(1)-Co(2)-O(4)	160.9(4)
O(6)-Co(1)-O(1W)	83.8(4)	N(2)-Co(2)-O(4)	95.2(3)

Symmetry transformations used to generate equivalent atoms: $^{\#1}$ y+1, -x+1, z; $^{\#2}$ –y+1, x-1, z; $^{\#3}$ x, y, -z.

Table S4. Selected bond distances (Å) and angles (deg) for **1-OH**.

Co(1)-O(10)$^{\#1}$	1.948(11)	O(2)-Co(1)-O(5)	90.7(2)
Co(1)-O(2)	2.017(5)	N(1)-Co(1)-O(5)	107.1(3)
Co(1)-N(1)	2.113(4)	N(2)-Co(1)-O(5)	86.8(2)
Co(1)-N(2)	2.138(5)	O(10)$^{\#1}$-Co(1)-O(4)	101.8(4)
Co(1)-O(5)	2.155(8)	O(2)-Co(1)-O(4)	90.1(2)
Co(1)-O(4)	2.339(6)	N(1)-Co(1)-O(4)	165.0(3)
Co(2)-O(9)$^{\#1}$	1.799(10)	N(2)-Co(1)-O(4)	99.4(2)
Co(2)-O(6W)	2.024(14)	O(5)-Co(1)-O(4)	58.0(3)
Co(2)-O(1)	2.063(6)	O(9)$^{\#1}$-Co(2)-O(6W)	161.5(7)
Co(2)-O(4)	2.089(9)	O(9)$^{\#1}$-Co(2)-O(1)	95.7(3)
Co(2)-O(5W)	2.163(13)	O(6W)-Co(2)-O(1)	87.8(5)
O(9)-Co(2)$^{\#2}$	1.798(10)	O(9)$^{\#1}$-Co(2)-O(4)	99.1(3)
O(10)$^{\#1}$-Co(1)-O(2)	96.1(3)	O(6W)-Co(2)-O(4)	98.8(5)
O(10)$^{\#1}$-Co(1)-N(1)	92.7(3)	O(1)-Co(2)-O(4)	93.6(2)
O(2)-Co(1)-N(1)	92.1(2)	O(9)$^{\#1}$-Co(2)-O(5W)	93.7(6)
O(10)$^{\#1}$-Co(1)-N(2)	90.7(2)	O(6W)-Co(2)-O(5W)	68.6(7)
O(2)-Co(1)-N(2)	166.9(2)	O(1)-Co(2)-O(5W)	83.0(4)
N(1)-Co(1)-N(2)	76.4(2)	O(4)-Co(2)-O(5W)	167.0(6)
O(10)$^{\#1}$-Co(1)-O(5)	158.9(4)		

Symmetry transformations used to generate equivalent atoms: $^{\#1}$ *y*, -*x*, *z*; $^{\#2}$ -*y*, *x*, *z*; $^{\#3}$ *x*, *y*, -*z*.